ELSEVIER

Quadrilateral mesh generation I : Metric based method

Wei Chen[a,d,e], Xiaopeng Zheng[a,d,e], Jingyao Ke[b], Na Lei[a,d,e,*], Zhongxuan Luo[a,d,e], Xianfeng Gu[c]

[a] *Dalian University of Technology, Dalian, China*
[b] *University of Science and Technology of China, Hefei, China*
[c] *Stony Brook University, NY, United States of America*
[d] *Key Laboratory for Ubiquitous Network and Service Software of Liaoning Province, Dalian, China*
[e] *DUT-RU Co-Research Center of Advanced ICT for Active Life, Dalian, China*

Highlights

- For any given locations and indices of singularities automatically produce quad mesh.
- Give sufficient and necessary conditions for a Riemannian Metric to be induced by a quad mesh.
- Based on Ricci Flow method, the existence and uniqueness are guaranteed.

Abstract

This work proposes a novel metric based algorithm for quadrilateral mesh generating. Each quad-mesh induces a Riemannian metric satisfying special conditions: the metric is a flat metric with cone singularities conformal to the original metric, the total curvature satisfies the Gauss–Bonnet condition, the holonomy group is a subgroup of the rotation group $\{e^{ik\pi/2}\}$, there is cross field obtained by parallel translation which is aligned with the boundaries, and its streamlines are finite geodesics. Inversely, such kind of metric induces a quad-mesh. Based on discrete Ricci flow and conformal structure deformation, one can obtain a metric satisfying all the conditions and obtain the desired quad-mesh.

This method is rigorous, simple and automatic. Our experimental results demonstrate the efficiency and efficacy of the algorithm.

1. Introduction

Quadrilateral meshes. With the development of 3D acquisition technologies, triangle meshes have become ubiquitous in many engineering fields for their simplicity and flexibility. However, quadrilateral meshes have been widely used in CAD and simulation because they have many merits: (1) a quad-mesh has tensor product structure, suitable for spline fitting. Hence a quad-mesh can be applied for high-order surface modeling, such as use of splines
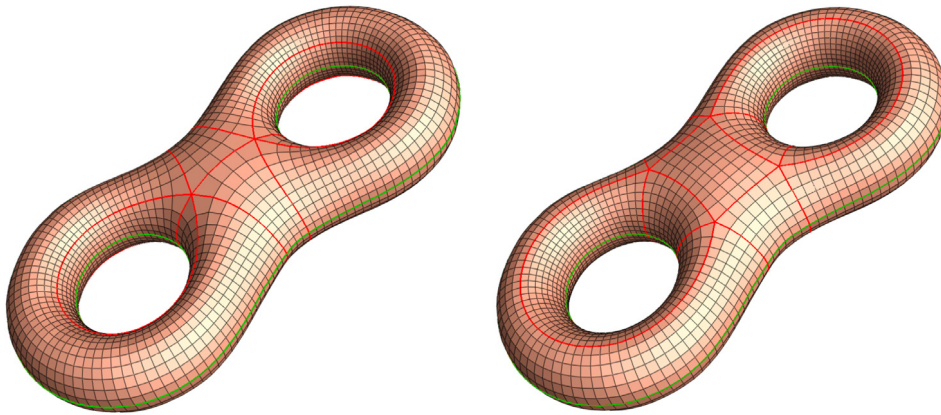

Fig. 1. A quad-mesh with 4 and 8 singularities on a genus two closed surface. The red curves are the separatrices, which form the skeletons. The green curves reflect the symmetry of the genus two closed surface. In general, the separatrices may not be the shortest tunnel loops of the quad mesh . (For interpretation of the references to color in this figure legend, the reader is referred to the web version of this article.)

and NURBS in CAD/CAM and subdivision surfaces in the movie industry; (2) a quad-mesh better captures the local geometric characteristics, such as principle directions or sharp features, as well as the semantics of the objects, hence it is widely used in animation industry; (3) patches of the skeleton of quad-meshes with a rectangular grid topology match the sampling pattern of textures. Therefore a quad-mesh is preferred for texture mapping and compression.

Fig. 1 shows two quad-meshes on a genus two closed surface. A vertex is called *regular*, if its topological valence is 4; otherwise, it is *singular*, where the valence of a vertex is the number of faces adjacent to the vertex. The left quad-mesh has 4 singularities, the right quad-mesh has 8 singularities. The *separatrices* are drawn in red, which are geodesics, roughly speaking the shortest paths on the quad-mesh, connecting singularities. The separatrices divide the surface into rectangular patches, this forms the *skeleton* of the quad-mesh, which is the coarsest level of the quad-mesh. The finer levels of the quad-mesh can be obtained by subdividing the skeleton.

The regularity of the quad-mesh can be described by the number of singularities, and the global behavior of the separatrices. Roughly speaking, quad-meshes can be classified to four categories with the ascending regularity:

1. Unstructured quad-mesh: a large fraction of its vertices are singularities, the tensor product structure can hardly be found.
2. Valence semi-regular quad-mesh: The number of singularities are few, but the separatrices have complicated global behavior; they may have intersections, form spirals and go through most edges.
3. Semi-regular quad-mesh: The separatrices divide the quad-mesh into several topological rectangles, the interior of each topological rectangle is a regular grid.
4. Regular quad-mesh: There are no singularities, all vertices are regular. A regular quad-mesh has strong topological restriction, it must be an annulus or a torus.

The current work focuses on a special class of quad-meshes, the semi-regular quad-mesh.

Metric based method. Given a topological surface S with a quad-mesh structure $\mathcal{Q}$, if we treat each quadrilateral face as a unit Euclidean square, then the quad-mesh structure naturally induces a Riemannian metric $\mathbf{g}$, which will be called the *quad-mesh metric*. The metric $\mathbf{g}$ induces zero Gaussian curvature everywhere, except at the singularities. If the topological valence of an interior singularity is k, then the Gaussian curvature measure at the point is $(1-k/4)\pi$; the Gaussian curvature measure of a boundary singularity with valence k is $(1 - k/2)\pi$. Therefore, the metric $\mathbf{g}$ is a flat metric with cone singularities.

In practice, it is highly desirable that the quad-faces are uniform squares. This implies that the quad-mesh metric $\mathbf{g}$ is *conformal* to the initial Euclidean metric, namely these two Riemannian metrics differ by a scalar function. In this work, we study the following problem:

Problem 1.1. Given a topological surface S, what kind of Riemannian metric $\mathbf{g}$ is induced by a quad-mesh $\mathcal{Q}$?

We prove that a metric **g** induced by a quad-mesh $\mathcal{Q}$ has many special properties:

1. The metric **g** is flat except at the singularities. The total curvature measures at the singularities equals to 2π multiply the Euler characteristic number of the surface. This is the *Gauss–Bonnet condition*.
2. In each quad-face, we can assign a cross (two orthogonal line segments, parallel to edges), then we get a global smooth *cross field*. This is equivalent to the so-called *holonomy condition*.
3. If the surface has boundaries, then the cross field is aligned with the boundaries, namely the boundaries are either parallel or orthogonal to the axes of the crosses. This is called *boundary alignment condition*.
4. If we connect the horizontal and vertical edges of the quad-faces, we get geodesic loops. If we subdivide the quad-mesh infinite many times, we obtain geodesic lamination, each leaf is a closed loop. This is called the *finite geodesic lamination condition*.

Inversely, if we have a metric **g** satisfying the above conditions, then the geodesics aligned with the cross field give the quad-mesh $\mathcal{Q}$.

Equivalently, the surface with the metric $(S, \mathbf{g})$ can be treated as a generalized translation surface.

Definition 1.2 (*Generalized Translation Surface*). Suppose P is a polygon immersed in the Euclidean plane $\mathbb{R}^2$. The sides of P are identified by the rigid motions of the plane, such that all the rotation angles are $k\pi/2$, $k \in \mathbb{Z}$, then the quotient space is called a generalized translation surface.

Fig. 13 shows a simple translation surface.

This fact inspires us to develop the metric driven approach for quad-mesh generation. In order to find a high quality quad-mesh $\mathcal{Q}$, we try to find a Riemannian metric **g** satisfying the above conditions, then trace the geodesics under **g**. First, we obtain a flat metric with cone singularities $\tilde{\mathbf{g}}$ using discrete Ricci flow method [1]. The Ricci flow theory guarantees the existence and the uniqueness of the solution. Then we deform the surface with the flat metric $\tilde{\mathbf{g}}$ to satisfy the above conditions. Once the metric is obtained, the geodesics can be calculated using exact geodesic tracing method on polyhedral surfaces [2]. Two families of orthogonal geodesics induce the quad-mesh $\mathcal{Q}$.

Contributions. To the best of our knowledge, this is the first method that generates quad-mesh by designing a Riemannian metric with special properties. The main Theorems 3.7 and 3.8 give the equivalence relation between a quad-mesh and its induced Riemannian metric. This gives a novel approach to construct the quad-mesh by finding the metric. Thanks to the solid theory of discrete surface Ricci flow [1], which guarantees the existence and uniqueness of the solution. The clean and succinct theoretic results make the algorithm pipeline simple and automatic.

The work is organized as follows: Section 2 briefly reviews the most related works; Section 3 introduces the theoretic background and proves the main theorems; Section 4 explains the algorithm in details, and give simple examples to illustrate the key ideas; the experimental results are reported in Section 5. Finally, the work concludes in Section 6.

2. Previous works

The literature of quad-meshing is vast, in the following we only review the most relevant works. For more complete and thorough literature review, we refer readers to [3]. There are several approaches for quad-mesh generation.

Triangle mesh to quad-mesh conversion. The simplest way is to convert a triangular mesh to a quad-mesh directly, then perform Catmull–Clark subdivision. Alternatively, two original adjacent triangles can be fused into one quadrilateral to form a quad-mesh [4–7]. This type method can only produce unstructured quad-meshes, the quad shape is determined by the input triangle mesh.

Patch based approach. This approach computes the skeleton first, which divides the input surface into several square patches, then subdivides the patches to obtain the quad-mesh. This method can produce semi-regular quad-meshes. The clustering method generates the skeleton by merge neighboring triangle faces into a patch, such as normal-based and center-based methods [8,9]. Poly-cube maps [10–13] are adopted to compute the patches.

Parameterization based approach. Many quad-meshing algorithms belong to this category. The spectral surface quadrangulation method [14,15] produces the skeleton structure from the Morse–Smale complex of an eigenfunction of the Laplacian operator on the input mesh. Discrete harmonic forms [16], periodic global parameterization [17] and branched coverings methods [18] are all based on parameterization for quad mesh generation.

Voronoi based method. The method in [19] generates quad-meshes by introducing Lp-Centroidal Voronoi Tessellation (Lp-CVT), which is a generalization of CVT that allows for aligning the axes of the Voronoi cells with a predefined background tensor field. This method can only produce non-structured quad-meshes; there is no global tensor product structure.

Cross field based method. Cross field guided quad-mesh generation was widely studied recently and many approaches have been proposed. Each approach must first choose a way to represent a cross, for example N-RoSy representation [20], period jump technique [21] and complex value representation [22]. Then the approaches usually generate a smooth cross field by an energy minimization technique. The typical measure of field smoothness is a discrete version of the Dirichlet energy [23]. In the end, based on the obtained cross field, these approaches generate the quad meshes by using streamline tracing techniques [24] or parameterization method [3].

The cross field guided quad mesh generation method can be very useful and flexible. However it is not easy to control the positions of the singularities and the structures of the quad layout directly. The work in [25] relates the Ginzburg–Landau theory with the cross field for genus zero surface case.

Comparing to all the existing methods, our method tackles the problem from a complete different angle — the Riemannian metric induced by the quad-mesh. By using discrete Ricci flow, such kind of metric can be obtained with theoretic guarantees.

3. Theoretic background

Definition 3.1 (*Quadrilateral Mesh*). Suppose S is a topological surface, $\mathcal{Q}$ is a cell partition of S, if all cells of $\mathcal{Q}$ are topological quadrilaterals, then we say $(S, \mathcal{Q})$ is a quadrilateral mesh.

Definition 3.2 (*Face Path*). A face path in $(S, \mathcal{Q})$ is a sequence $\gamma = (\sigma_0, \sigma_1, \ldots, \sigma_n)$ such that $\sigma_0, \sigma_1, \ldots, \sigma_n$ are faces and two consecutive faces σ_i and σ_{i+1} are neighbors in $\mathcal{Q}$ for all $0 \leq i \leq n$.

The *inverse path* of γ is denoted by $\gamma^{-1} = (\sigma_n, \sigma_{n-1}, \ldots, \sigma_0)$. We write $\gamma\eta$ for the concatenation of γ with some face path $\eta = (\sigma_n, \ldots, \sigma_m)$. The face path γ is *closed* if $\sigma_0 = \sigma_n$.

Each face path $\gamma = (\sigma_0, \ldots, \sigma_n)$ in K induces a piecewise linear path $\bar{\gamma}$ in the geometric realization of $(S, \mathcal{Q})$: Join the barycenter of each face σ_i by linear paths to the barycenters of the common edges $\sigma_i \cap \sigma_{i-1}$ and $\sigma_i \cap \sigma_{i+1}$ of the neighboring faces σ_{i-1} and σ_{i+1}, respectively. The face path γ is closed if and only if the induced piecewise linear path $\bar{\gamma}$ is closed. Often we identify γ with $\bar{\gamma}$. Moreover, we write $[\gamma]$ for the homotopy class of $\bar{\gamma}$ with endpoints fixed.

On a quad-mesh, the *topological valence* of a vertex is the number of faces adjacent to the vertex.

Definition 3.3 (*Singularity*). Suppose $(S, \mathcal{Q})$ is a quadrilateral mesh. If the topological valence of an interior vertex is 4, then we call it a *regular vertex*, otherwise a *singularity*; if the topological valence of a boundary vertex is 2, then we call it a *regular boundary vertex*, otherwise a *boundary singularity*. The index of a singularity is defined as follows:

$$\mathrm{Ind}(v_i) = \begin{cases} 4 - \mathrm{Val}(v_i) & v_i \notin \partial(S, \mathcal{Q}) \\ 2 - \mathrm{Val}(v_i) & v_i \in \partial(S, \mathcal{Q}) \end{cases}$$

where $\mathrm{Ind}(v_i)$ and $\mathrm{Val}(v_i)$ are the index and the topological valence of v_i.

3.1. Topological structure

Parallel transport and holonomy.

Definition 3.4 (*Quadrilateral Mesh Metric*). Given a quadrilateral mesh $(S, \mathcal{Q})$, each quadrilateral face is assigned with the Euclidean metric to be a canonical unit square. This induces a flat metric with cone singularities, denoted as **g** and called as the quadrilateral mesh metric of $(S, \mathcal{Q})$.

Under the quad-mesh metric, the surface is flat, except at the singularities. Let Γ be the set of all singularities, then $(S - \Gamma, \mathbf{g})$ is flat everywhere. Hence the parallel transportation under $\mathbf{g}$ in $(S - \Gamma, \mathbf{g})$ is equivalent to the translation in the Euclidean space.

Definition 3.5 (*Parallel Transportation*)**.** Given a quadrilateral mesh $(S, \mathcal{Q})$ with the quad-mesh metric $\mathbf{g}$, $\gamma = (\sigma_0, \sigma_1, \ldots, \sigma_{n-1}, \sigma_n)$ is a face path, suppose $\mathbf{v}$ is a tangent vector in σ_0, at the ith step, $i = 1, 2, \ldots, n$, both σ_{i-1} and σ_i are isometrically embedded on the Euclidean plane sharing a common edge, then the tangent vector is translated from σ_{i-1} to σ_i. Eventually the tangent vector reaches the σ_n. The result vector is defined as the parallel transportation of $\mathbf{v}$ along the face path γ.

Definition 3.6 (*Holonomy*)**.** Suppose $(S, \mathcal{Q})$ is a quad-mesh with singularity set Γ and the quad-mesh metric $\mathbf{g}$. Let $\gamma = (\sigma_0, \sigma_1, \ldots, \sigma_{n-1})$ be a face loop.   Suppose one chooses an orthonormal frame $\{\mathbf{e}_1, \mathbf{e}_2\}$ in σ_0, where $\mathbf{e}_k$'s are parallel to the edges of σ_0, and parallel transport the frame along γ. When the transportation returns to σ_0 again, the frame becomes $\{\tilde{\mathbf{e}}_1, \tilde{\mathbf{e}}_2\}$. The rotation from the initial frame to the final frame is called the *holonomy* of γ, and denoted as $\langle \gamma \rangle$.

Because $(S - \Gamma, \mathbf{g})$ is flat everywhere, if γ_1 and γ_2 are homotopic to each other in $S - \Gamma$, then their holonomies are equal, $\langle \gamma_1 \rangle = \langle \gamma_2 \rangle$. The planar rotation group is denoted as $\mathcal{R} = \{e^{k\pi/2}, k = 0, 1, 2, 3\}$. This induces a homomorphism from the fundamental group of $S - \Gamma$ to the rotation group, $\varphi : [\gamma] \to \langle \gamma \rangle$

$$\varphi : \pi_1(S - \Gamma, \sigma_0) \to \mathcal{R}, \tag{1}$$

where σ_0 is a fixed face. The mapping φ is called the *holonomy homomorphism* of the quad-mesh. The image of the holonomy homomorphism

$$\Pi(\mathcal{Q}, \sigma_0) := \varphi(\pi_1(S - \Gamma, \sigma_0))$$

is called the *holonomy group* of the quad-mesh. For any face loop γ, its holonomy $\langle \gamma \rangle$ is a rotation with angle $k\pi/2$, where k is an integer. Therefore, the order of the holonomy group $\Pi(\mathcal{Q}, \sigma_0)$ is at most 4.

3.2. Riemannian metric structure

The quad-metric has many special properties, which are summarized as the following theorem.

Theorem 3.7 (*Quad-mesh Metric*)**.** *If a Riemannian metric $\mathbf{g}$ with cone singularities is induced by a quad-mesh $(S, \mathcal{Q})$, then it has the following properties:*

1. *The metric $\mathbf{g}$ is flat except at the singularities. The total curvature measures at the singularities equals to 2π multiply the Euler characteristic number of the surface. This is the* Gauss–Bonnet condition.
2. *In each quad-face, we can assign a cross (two orthogonal line segments, parallel to edges), then we get a global smooth* cross field. *Namely, the holonomy group is a subgroup of $\mathcal{R}$. This is equivalent to the* holonomy condition.
3. *If the surface has boundaries, then the cross field is aligned with the boundaries, namely the boundaries are either parallel or orthogonal to the axes of the crosses. This is called* boundary alignment condition.
4. *By connecting the horizontal or vertical edges of the quad-faces, geodesic loops can be obtained. If the quad-mesh is subdivided infinite many times, a geodesic lamination is obtained, whose leaves are closed loops. This is called the* finite geodesic lamination condition.

Proof. *Gauss–Bonnet condition* Each regular vertex has 0 curvature. Each singular vertex has curvature measure $Ind(v_i)\frac{\pi}{2}$, the total Gaussian curvature satisfies the Gauss–Bonnet theorem:

$$\sum_{v_i} Ind(v_i)\frac{\pi}{2} = 2\pi \chi(S).$$

Holonomy Condition The holonomy group of the quad-mesh is a subgroup of $\mathcal{R}$. A cross is invariant under the $\mathcal{R}$ action. We can put a cross at the base face σ_0, whose two axes are aligned with the edges of the square, and parallel transport to all the faces. This gives a global smooth cross field.
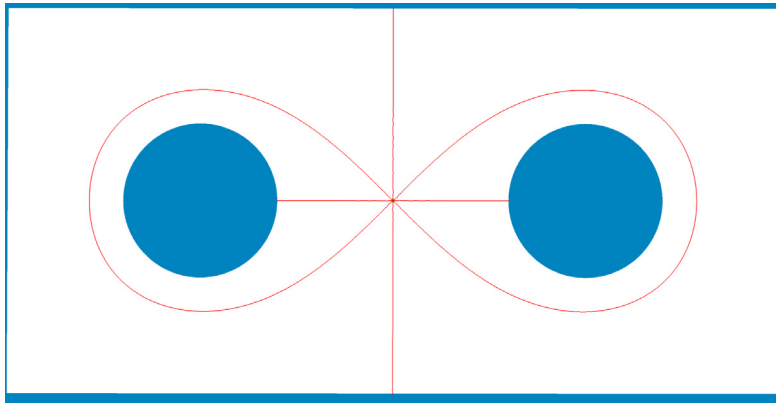
Fig. 2. Gauss–Bonnet condition: a planar domain with two inner boundaries. The center singularity is with index -4, everywhere else the curvature is 0. The geodesic curvature along the boundaries are also 0. The geodesics through the singularity are drawn as red curves . (For interpretation of the references to color in this figure legend, the reader is referred to the web version of this article.)

Boundary Alignment All the boundaries of the quad-mesh consists of the edges of square faces, therefore the cross axes are parallel or orthogonal to the boundaries.

Finite Geodesic lamination We start from the center of a face, issue a geodesic parallel with the edges of the face. The geodesic will not enter the same face more than two times. The number of faces is finite, therefore, the geodesic is of finite length. This holds for all the geodesics constructed this way. □

Theorem 3.8 (*Inverse Quad-mesh Metric Theorem*). *Given a topological surface S and a flat metric* **g** *with cone singularities* γ, **g** *has the following properties:*

1. *The metric* **g** *is flat except at the singularities. The total curvature measures at the singularities equals to* 2π *multiply the Euler characteristic number of the surface. This is the* Gauss–Bonnet condition.
2. *The holonomy group is a subgroup of* $\mathcal{R}$. *This is the* holonomy condition.
3. *There is a cross field obtained by parallel transporting a cross defined at a point* $p \in S - \Gamma$, *such that the cross field is aligned with the boundaries. This is the* boundary alignment condition.
4. *The stream lines parallel to the cross field are finite geodesic loops. This is the* finite geodesic lamination condition.

Then a quadrilateral mesh can be constructed on S, such that the quad-mesh metric is **g**.

Proof. If we have a metric **g** that satisfies the above conditions, then the geodesics aligned with the cross field give the quad-mesh $\mathcal{Q}$. The geodesics through the singularities are the separatrices. □

As shown in Fig. 2, given a planar rectangle with two circular holes, a special flat metric is computed with a single singularity, whose index is -4. The curvature is 0 every where else, including the boundaries. Therefore, the total curvature is -2π, the Euler characteristic number is -1, the Gauss–Bonnet formula holds. The red curves are geodesics through the singularity, they are perpendicular to the boundaries, or form geodesic loops. They are either parallel or orthogonal to each other.

Fig. 3 shows the holonomy condition. The quad-mesh is depicted by checker-board texture mapping. Each checker represents a quadrilateral face. The parallel transportation along two inner boundaries induces trivial holonomy. Similarly, the holonomy of the loop surrounding the singularity is also trivial.

Fig. 4 shows the boundary alignment condition. We put a cross in each face, whose axis is aligned with the edges, then we obtain a smooth cross field. The cross field is aligned with all the boundaries.

Fig. 5 shows the finite geodesic condition. All the geodesics parallel to the edges of the faces either terminate at the boundaries or the singularity, or form loops.

Fig. 6 illustrates the same surface with 2 valence-6 singularities, each has $-\pi$ Gaussian curvature measure. From left to right, the quad-mesh, the cross field, the geodesics, the singularities and the geodesics through them and perpendicular to the boundaries. The flat metric with the cone singularities satisfies all the 4 conditions.
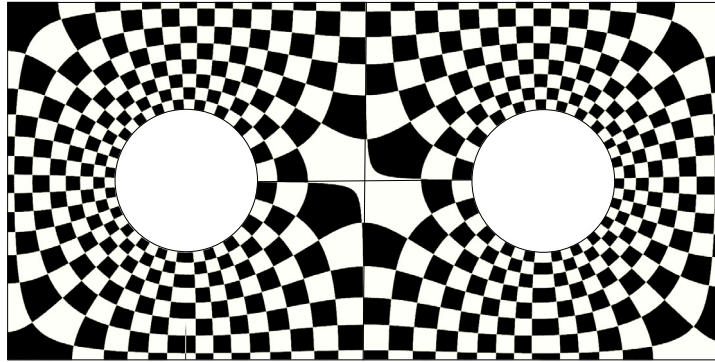
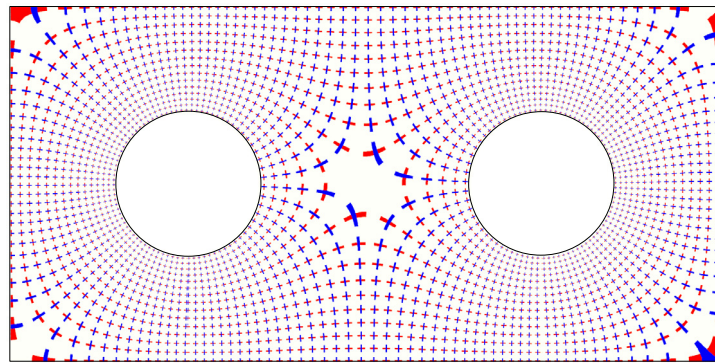**Fig. 3.** Holonomy condition: the holonomy group of the quad-mesh is trivial.

Fig. 4. Boundary alignment condition: the cross field is aligned with all the boundaries.
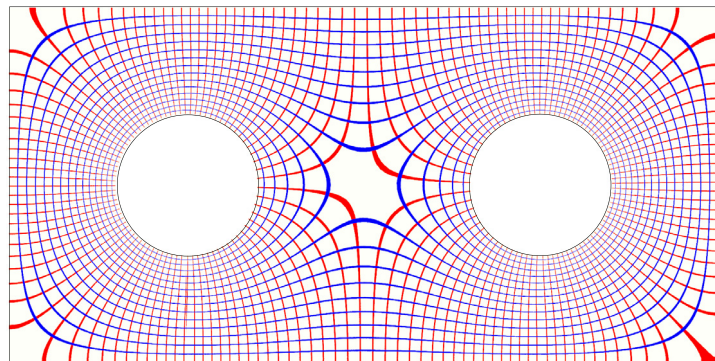

Fig. 5. Finite geodesic condition: all the geodesics aligned with the cross field are finite.

Fig. 7 shows the same surface with 4 valence-5 singularities, each has $-\frac{\pi}{2}$ Gaussian curvature measure. The flat metric with cone singularities satisfies all the 4 conditions.

Fig. 8 shows the same surface with different positions of singularities, the flat metric **g** satisfies the Gauss–Bonnet condition. The global smooth cross field in the 2nd frame shows the metric satisfies the holonomy condition. But the cross fields are not aligned with the inner boundaries, hence the geodesics are not parallel or orthogonal to the inner boundaries as shown in the 3rd frame.
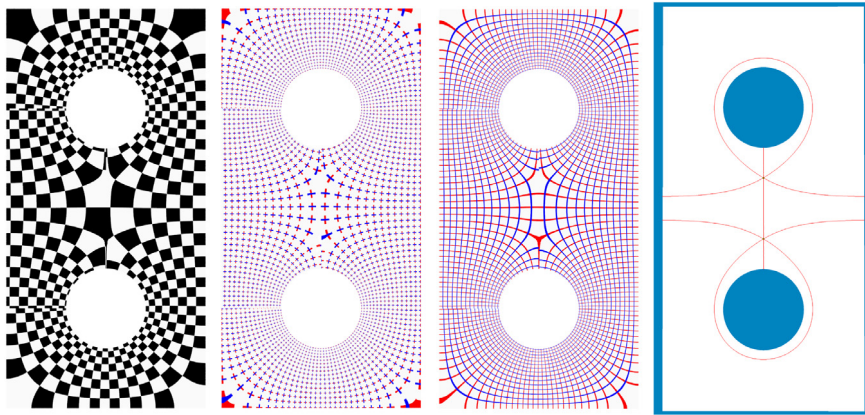
Fig. 6. Two singularity configuration, corresponding to a holomorphic quadratic form.
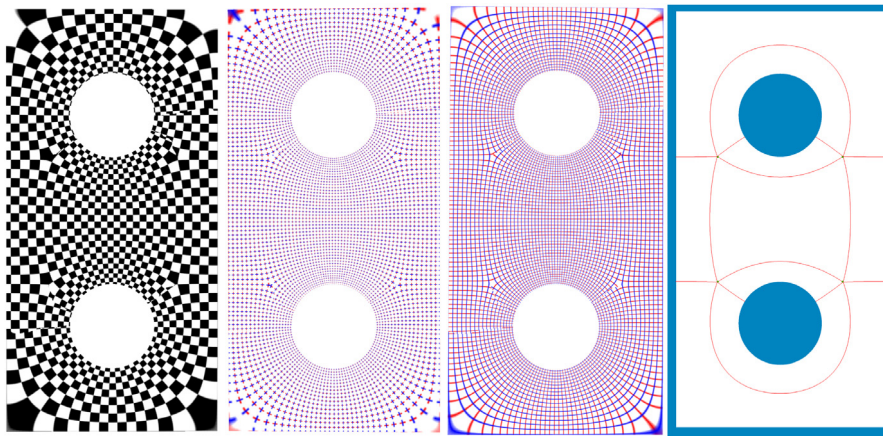

Fig. 7. Four singularity configuration, corresponding to a holomorphic quartic form.
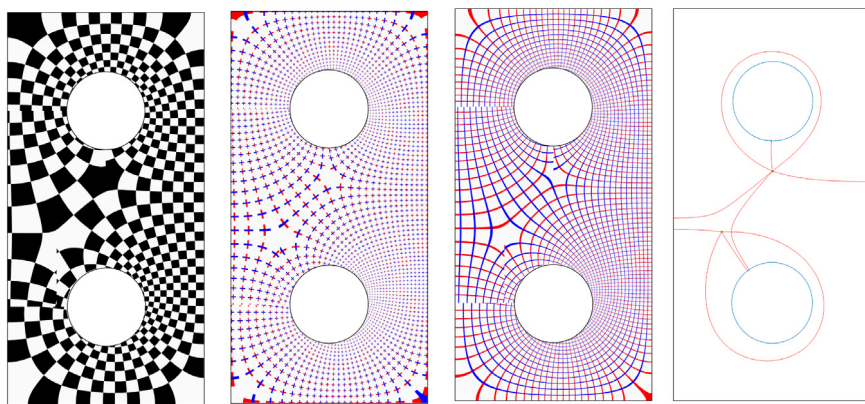

Fig. 8. Two singularity configuration, violating the boundary alignment condition.

Lemma 3.9. *Suppose S is a genus zero surface, $\mathbf{g}$ is a flat metric with internal cone singularities $\Gamma_1 = \{p_1, p_2, \ldots, p_n\}$; along the boundary components there are boundary singularities $\Gamma_2 = \{q_1, q_2, \ldots, q_m\}$, where the discrete Gaussian curvature measure of p_i is $\frac{k_i}{2}\pi$, where $k_i \in \mathbb{Z}$ is an integer, the curvature measure of q_j is*
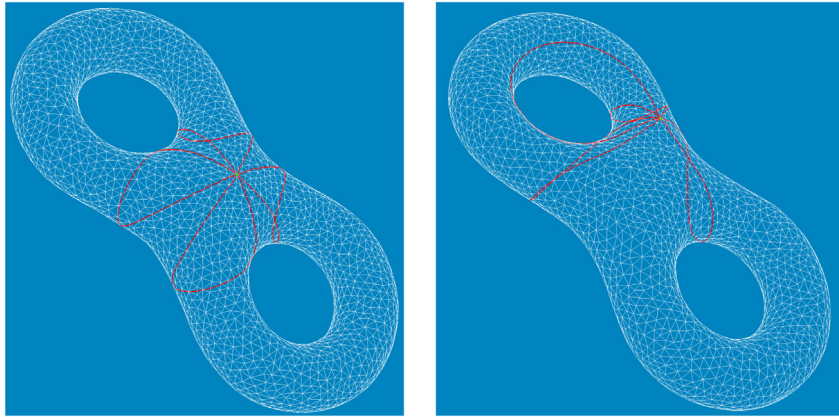
Fig. 9. A flat metric with a cone singularity, whose curvature measure is -4π. The metric violates the holonomy condition.

$\frac{l_j}{2}\pi$, $l_j \in \mathbb{Z}$. Furthermore **g** satisfies the Gauss–Bonnet condition,

$$\sum_{i=1}^{n} k_i + \sum_{j=1}^{m} l_j = 4\chi(S),$$

then **g** also satisfies the holonomy condition.

Proof. Suppose the boundary components of the surface S are

$$\partial S = s_0 - s_1 \cdots s_t,$$

and the singularity set is $\Gamma = \{p_1, p_2, \ldots, p_n\}$. Let α_j is the loop around p_j, then the fundamental group of the surface is given by

$$\pi_1(S - \Gamma_1) = \langle s_1, s_2, \ldots, s_t, \alpha_1, \ldots, \alpha_n \rangle.$$

The holonomies of the generators

$$\langle \alpha_i \rangle = \frac{k_i}{2}\pi,$$

the holonomy of each boundary component s_j equals to the total Gaussian curvature measures of all corner singularities along s_j. Hence, the metric satisfies the holonomy condition. $\square$

But if the surface is of high genus, then a flat metric **g** satisfying Gauss–Bonnet may not satisfy the holonomy condition. Fig. 9 shows a metric satisfies the Gauss–Bonnet condition, but violates the holonomy condition. We use discrete Ricci flow method to compute a flat metric **g** on a genus two surface, such that the unique singularity p is with -4π Gaussian curvature. According to the discrete uniformization theorem proved in [1], such kind of metric exists and is unique up to scaling. We calculate several geodesic loops through the singularity p. Suppose γ is a geodesic loop, $\gamma(0) = \gamma(1) = p$. If the metric **g** satisfies the holonomy condition, then the angle between two tangent vectors $\gamma'(0)$ and $\gamma'(1)$ is $\frac{k}{2}\pi$ under **g**, where k is an integer. We measure such angles of several geodesic loops through p, most of them are not $\frac{k}{2}\pi$. Hence the metric **g** does not satisfy the holonomy condition.

4. Algorithm

The metric based quad-mesh generation aims at computing a flat cone metric with singularities, satisfying the condition in Theorem 3.7, then finds two families of orthogonal geodesics to generate the quadrilateral mesh.

Algorithmic pipeline

Suppose the input surface S is discretized as a triangular mesh. The algorithm pipeline is as follows:

1. Determine the positions and indices of singularities Γ;
2. Compute a flat metric $\mathbf{g}_0$ with cone singularities using discrete surface Ricci flow algorithm;
3. Compute a cut graph L of the surface, such that $S - L$ is a topological disk. Furthermore, for each singularity $v_i \in \Gamma$, find the shortest path connecting v_i and the boundary of $S - L$, the shortest paths are added to L;
4. Isometrically immerse $(S - L, \mathbf{g}_0)$, the image is a planar immersed polygon P. Each pair of conjugate boundary segments of the polygon differ by a planar rigid motion.
5. Conformal structure deformation. Adjust the boundary of P, such that each pair of conjugate boundary segments of P differ by a translation and a rotation in $\mathcal{R}$, and all the boundary segments of S are horizontal or vertical. Use harmonic map to deform the interior of P. This induces a new flat metric $\mathbf{g}$, and a cross field ω satisfying the boundary condition.
6. Compute geodesics under $\mathbf{g}$ align the cross field ω. The geodesics through the singularities defines the skeleton, further subdivisions of the skeleton give the quad-mesh.

In the following, we explain each step in details.

4.1. Singularity location

The most crucial step of the algorithm pipeline is to determine the positions and indices of the singularities. One way is to manually input the positions and indices using heuristics, then generate the skeleton. In general, the singularity configurations need to be adjusted in order to improve the mesh quality.

An automatic way to determine the singularities is to use the poles and zeros of an Abelian differential on the surface. The details will be introduced in our later submission [26].

4.2. Discrete surface Ricci flow

Given a polyhedral surface with a triangulation, the surface has induced Euclidean metric, namely, a triangle mesh M.

Each face is a Euclidean triangle $[v_i, v_j, v_k]$ with edge lengths $\{l_i, l_j, l_k\}$. The corner angles and the edge lengths satisfies the cosine law:

$$l_i^2 = l_j^2 + l_k^2 - 2l_j l_k \cos \theta_i.$$

The discrete vertex Gaussian curvature is defined as angle deficit,

$$K(v_i) = \begin{cases} 2\pi - \sum_{jk} \theta_i^{jk} & v_i \notin \partial M \\ \pi - \sum_{jk} \theta_i^{jk} & v_i \notin \partial M \end{cases}$$

The total Gaussian curvature satisfies the Gauss–Bonnet theorem,

$$\sum_i K(v_i) = 2\pi \chi(M).$$

We associate each vertex v_i with a discrete conformal factor u_i, then the vertex scaling operator is defined as

$$l_{ij} = e^{u_i} \beta_{ij} e^{u_j},$$

where l_{ij} is the length of the edge $[v_i, v_j]$, β_{ij} is the initial edge length. Given target curvature $\bar{K} : V \to \mathbb{R}$, the discrete Ricci flow is defined as

$$\frac{du_i}{dt} = \bar{K}_i - K_i.$$

During the flow, the triangulation is updated to be Delaunay. Discrete Ricci flow is the gradient flow of the convex energy,

$$E(u_1, u_2, \ldots, u_n) = \int_0^{(u_1,\ldots,u_n)} \sum_{i=1}^{n} (\bar{K}_i - K_i) du_i.$$

This energy can be optimized using Newton's method.

For more details about the theory and algorithm of discrete Ricci flow, we refer readers to [27].

4.3. Cut graph

Given a triangle mesh M with singularities, the singularity set is denoted as Γ. First, we compute the cut graph G of the mesh M.

Let $\bar{M}$ be the dual mesh of M, then we compute a spanning tree $\bar{T}$ of $\bar{M}$. The cut graph G is defined as

$$G := \{e \in M | \bar{e} \notin \bar{T}\},$$

then $M - G$ is a topological disk. For each singularity $p_k \in \Gamma$, find the shortest path γ_k from p_k to the cut graph, then

$$L = G \bigcup_{p_i \in} \gamma_i$$

$\tilde{M} = M - L$ is a topological disk.

The cut graph algorithm can be applied to surfaces with boundaries by only operating on dual edges and faces not relating to edges or vertices on the primal boundary.

4.4. Isometric immersion

We can isometrically immerse $\tilde{M}$ with the flat metric $\mathbf{g}$ onto the plane [27], the immersion is denoted as $\varphi : \tilde{M} \to \mathbb{R}^2$. Then φ assigns planar coordinates for each vertex in $\tilde{M}$.

Each triangle face of $\tilde{M}$ corresponds to a face of M, each vertex $\tilde{v}_i \in \tilde{M}$ corresponds to a unique vertex $v_j \in M$. This defines a simplicial projection map $\psi : \tilde{M} \to M$, which is a covering map.

Each face f_i consists of three vertices, the face-vertex pair (f_i, v_j) represents the corner in f_i with v_j as the apex. Then the corners of $\tilde{M}$ and those of M have one-to-one correspondence. In the covering mesh $\tilde{M}$, we define the texture coordinates of a corner (f_i, v_j) as the texture coordinates of the vertex v_j. In the base mesh M, the texture coordinates of a corner equal to the texture coordinates of its preimage, $\psi^{-1}((f_i, v_j))$.

The $\tilde{M}$ represents one fundamental domain of the branched covering space of M, ψ represents the covering map from the covering space to the base surface. By abusing the notation, we use ψ to represent its restriction on $\tilde{M}$.

4.5. Conformal structure deformation

Let $e_{ij} \in M$ be an edge, it is adjacent to two faces $f_k = [v_i, v_j, v_k]$ and $f_l = [v_j, v_i, v_l]$, the chart transition mapping $\varphi_{ij} : \mathbb{R}^2 \to \mathbb{R}^2$ satisfies the condition

$$\varphi_{ij}(\varphi(f_k, v_i)) = \varphi(f_l, v_i), \varphi_{ij}(\varphi(f_k, v_j)) = \varphi(f_l, v_j).$$

The chart transition mappings are identity on edges not in L.

Consider the graph $L \subset M$, each vertex $v_i \in L$ has a topological valence in L, which is the number of edges in L and adjacent to v_i. We call vertices in L with valence 2 as regular vertices, otherwise as *nodes*. The nodes divide the graph L into *segments*. Each τ_i is a segment, the boundary ∂M is divided into segments, denoted as $\{\tau_1, \tau_2, \ldots, \tau_k\}$.

In $\tilde{M}$, the preimage of L becomes the boundary $\partial \tilde{M}$. Each γ_i has two preimages, denoted as $\tilde{\gamma}_i^+$ and $\tilde{\gamma}_i^-$, each τ_j has a unique preimage $\tilde{\tau}_j$. $\varphi(\tilde{\gamma}_i^+)$ and $\varphi(\tilde{\gamma}_i^-)$ differ by a planar rigid motion.

We can modify the coordinates of $\varphi(\tilde{\gamma}_i^+)$, $\varphi(\tilde{\gamma}_i^-)$, and $\varphi(\tilde{\tau}_j)$ by rotation and translation, such that
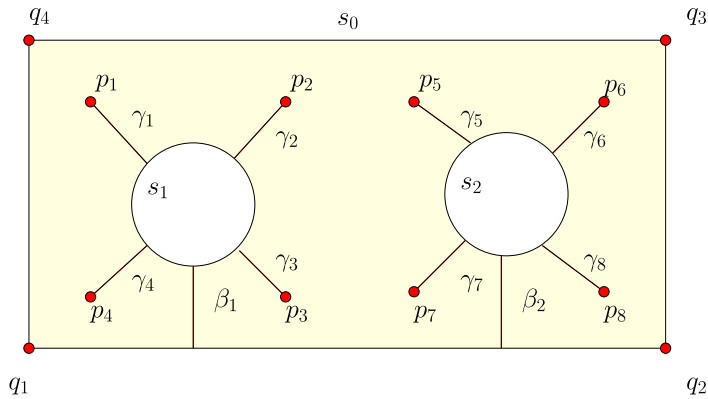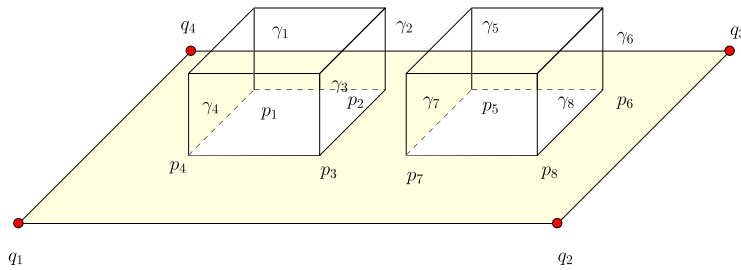
Fig. 10. Schematic layout.

Fig. 11. Desired flat metric with cone singularities.

- all $\varphi(\tilde{\tau}_j)$'s are horizontal or vertical;
- $\varphi(\tilde{\gamma}_i^+)$ and $\varphi(\tilde{\gamma}_i^-)$ differ by a translation and a rotation in $\mathcal{R}$.

After modifying the boundary coordinates to a planar rectangle, we calculate the coordinates of the interior vertices of $\tilde{M}$ using a harmonic map. The new local coordinates give a new Riemannian metric $\mathbf{g}$, which satisfies the holonomy condition and the boundary alignment condition.

4.6. Tracing geodesics

We compute the exact geodesic on polyhedral mesh with the metric $\mathbf{g}$ using the algorithm in [2]. First, we compute the geodesics issued from the singularities, which are orthogonal to the boundaries, or connected with other singularities. We call these special geodesics as *critical trajectories*.

The critical trajectories are the separatrices, which partition the surface into Euclidean rectangles under the metric $\mathbf{g}$. These rectangles are the coarsest level of the quad-mesh, or the *skeleton* of the quad-mesh. Then we subdivide the skeleton to form the refined quad-mesh.

4.7. One computational example

We use a simple example to illustrate the basic computation pipeline.

1. Singularity allocation and cut graph Fig. 10 shows a schematic 2D layout of a planar domain Ω, a rectangle with two circular holes. The domain has three boundary components, $\{s_0, s_1, s_2\}$, where s_0 is the exterior boundary component, s_1, s_2 are inner boundary components.

Fig. 11 shows the desired target metric with cone singularities. Following the design, eight interior singularities are manually assigned, $\{p_1, p_2, p_3, p_4, p_5, p_6, p_7, p_8\}$, the valences of them are 5. Four boundary singularities (corner points) are prescribed, $\{q_1, q_2, q_3, q_4\}$, their valences are 1.
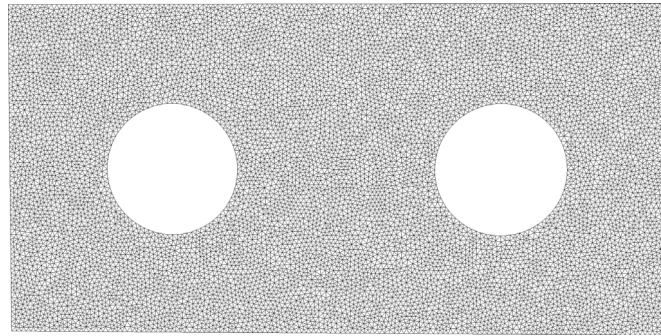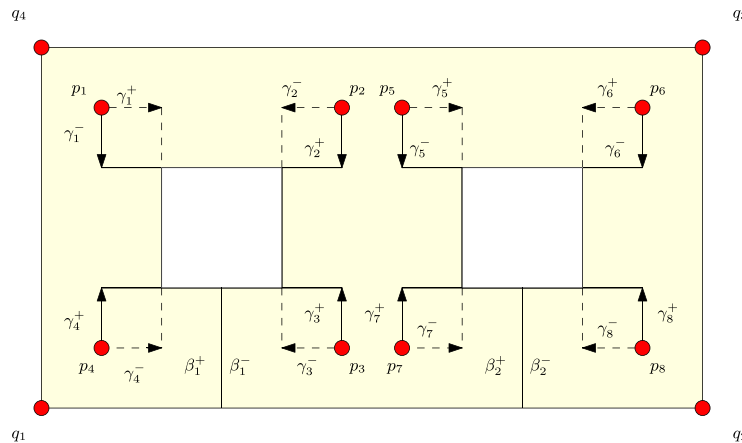
Fig. 12. Triangular mesh.

Fig. 13. Isometric immersion.

Fig. 10 also shows the cut graph L. From each interior singularity p_k to the inner boundary, we compute a shortest path γ_k. From each inner boundary component s_k to the exterior boundary s_0, we draw a shortest path β_k.

2. Ricci flow for flat metric with cone singularities Fig. 12 shows the triangular mesh of the domain, denoted as M. We use conventional planar mesh generation method to triangulate the planar domain Ω using gmsh [28], all the inner singularities are constrained to be vertices of the triangular mesh.

We use discrete surface Ricci flow algorithm [27] to compute a flat metric with cone singularities at the singularities, where

$$K(p_i) = -\frac{\pi}{2}, \, K(q_j) = \frac{\pi}{2}.$$

The flat metric is denoted as **g**.

3. Isometric immersion and deformation The surface $(\Omega, \mathbf{g})$ can be isometrically embedded in $\mathbb{E}^3$ as shown in Fig. 11. We slice $(\Omega, \mathbf{g})$ along the cut graph $L = \bigcup_i \gamma_i \bigcup_j \beta_j$ to obtain $\tilde{\Omega}$, which is a topological disk. Each γ_k is split into two boundary segments γ_k^+ and γ_k^-, similarly each β_k is split into β_k^+ and β_k^-. Then we isometrically flatten $\tilde{\Omega}$ to obtain an isometric immersion as shown in Fig. 13, the immersion is denoted as $\varphi : \tilde{\Omega} \to \mathbb{R}^2$.

In this example, the singularities are carefully chosen, so that the metric **g** satisfies the all conditions in Theorem 3.7, γ_k^+ and γ_k^- differ by a rotation of $\pi/2$, β_k^+ and β_k^- differ by translations. Hence, the conformal structure deformation is skipped.

We use the immersion φ as the texture coordinates for texture mapping, see Fig. 14. On the texture mapping image, we can see the horizontal and vertical geodesics.
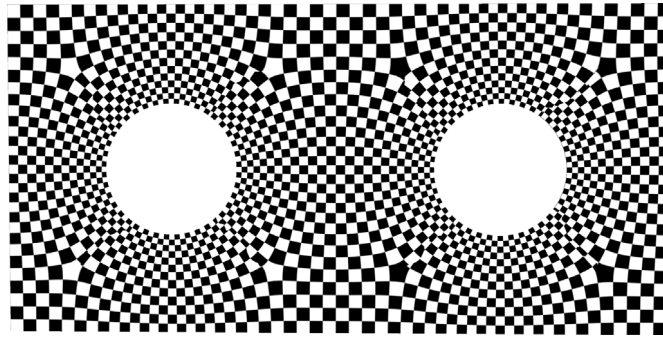
Fig. 14. Holomorphic quartic differential visualized by Checker board texture mapping.
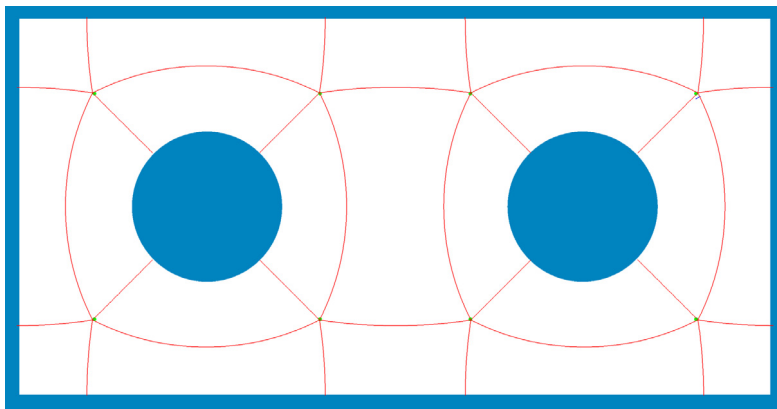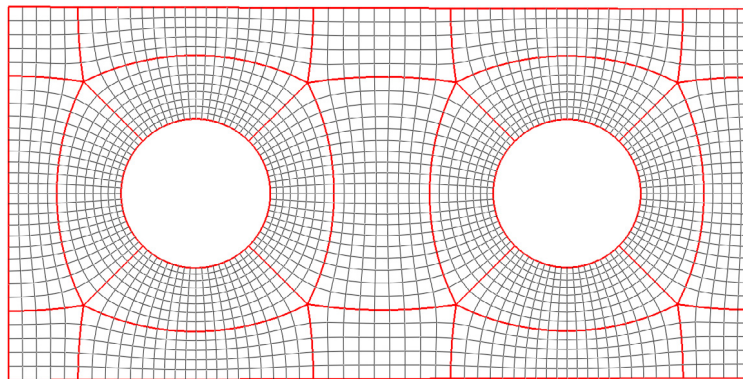

Fig. 15. Critical geodesics.

Fig. 16. The quad-mesh induced by geodesics.

4. Geodesics and quad-meshing The critical geodesics are traced, which either connect different singularities, or orthogonal to the boundaries. The critical geodesics give the skeleton of the quad-mesh as shown in Fig. 15.

We then refine the skeleton by tracing more geodesics on $(\Omega, \mathbf{g})$, which are orthogonal or parallel to the critical geodesics. The geodesics induce the quadrilateral meshing as shown in Fig. 16.
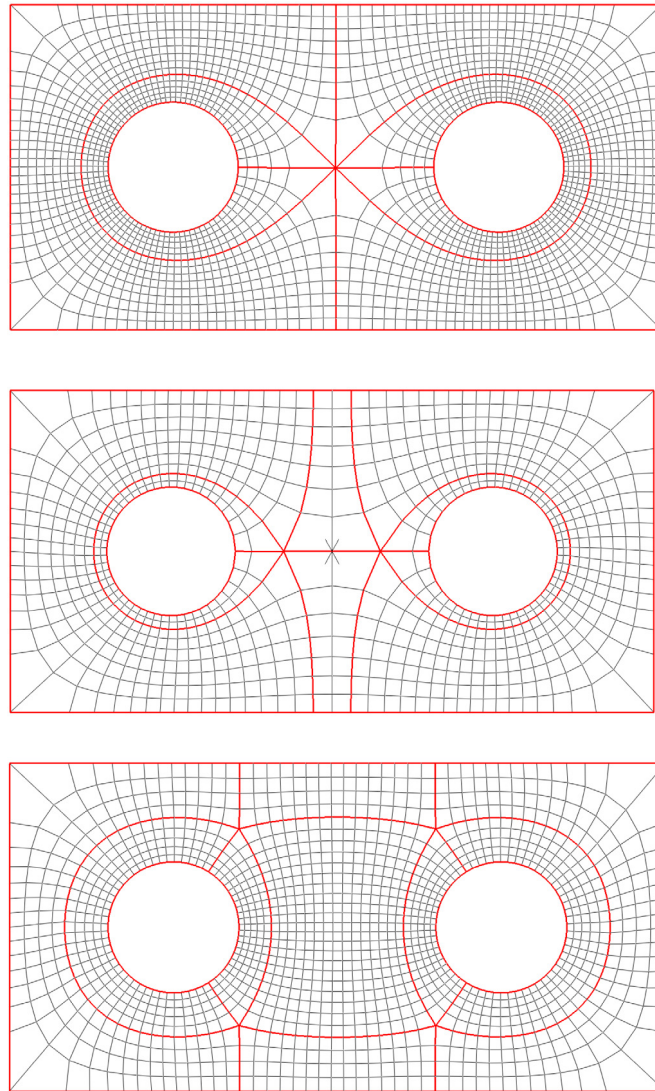
Fig. 17. A quad-mesh with 1, 2 and 4 singularities on a planar rectangle with 2 circular inner holes.

5. Experimental results

All the experiments were conducted on a PC with 1.90 GHz Intel(R) core(TM) i7-8650U CPU and 64-bit Windows 10 operating system. The running time is reported in Table 1.

Fig. 17 illustrates the quad-meshes obtained by the proposed method with different number of singularities of the planar rectangle with two circular inner holes.

The proposed method can be applied for surfaces with arbitrary typologies. Figs. 1 and 18 show the quad-meshes with different number of singularities of a genus two closed surface.

The computation of triangular mesh generation, Ricci flow, tracing critical trajectories (and generating skeletons) are fast enough to allow the users to modify the singularity positions interactively. The geodesic tracing is accurate and stable, so the computation of skeletons is straightforward without any manual refinement. Therefore, the whole computational pipeline is automatic except the initial step for singularity location and the connectivity establishment of the separatrices between singularities.
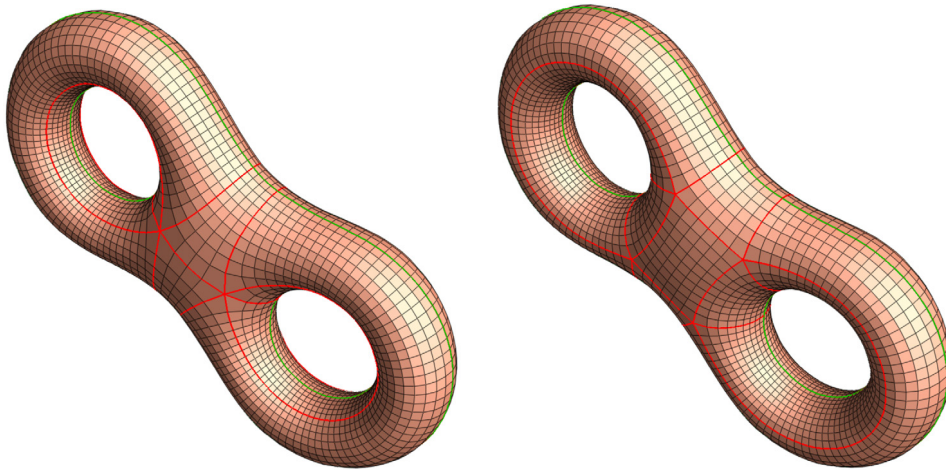
Fig. 18. A quad-mesh with 4 and 8 singularities on a genus 2 surface.

Table 1
Computational time.

Model	# Vertices	# Singularities	Time (ms)
Rectangle with holes	10 529	1	30 936
Rectangle with holes	10 675	2	40 753
Rectangle with holes	10 641	4	24 510
Rectangle with holes	10 668	12	18 733
Eight mesh	16 061	4	14 988
Eight mesh	16 060	8	12 427

6. Conclusion

A novel quadrilateral meshing algorithm is introduced, which is based on constructing Riemannian metrics with special properties. We show a quad-mesh induces a flat metric with cone singularities satisfying the curvature condition, holonomy condition, boundary alignment condition, and finite geodesic condition as specified in Theorem 3.7. Inversely, such kind of metric induces a quad-mesh.

By using discrete surface Ricci flow and conformal structure deformation algorithms, we can obtain such kind of metrics, and in turn construct quad-meshes. Our experimental results demonstrate that the method is theoretically rigorous, practically simple and automatic.

In future, we will explore the methods to automatically determine the positions and indices of all the singularities based on Riemann–Roch theory and Abelian differentials.

Acknowledgments

References

[1] Xianfeng David Gu, Feng Luo, Jian Sun, Tianqi Wu, A discrete uniformization theorem for polyhedral surfaces, ACM Trans. Graph. 109 (2) (2018) 223–256.
[2] Vitaly Surazhsky, Tatiana Surazhsky, Danil Kirsanov, Steven J. Gortler, Hugues Hoppe, Fast exact and approximate geodesics on meshes, ACM Trans. Graph. 24 (3) (2005) 553–560.
[3] David Bommes, Bruno Lévy, Nico Pietroni, Enrico Puppo, Claudio Silva, Marco Tarini, Denis Zorin, Quad-mesh generation and processing: A survey, Comput. Graph. Forum 32 (6) (2013) 51–76.

[4] Topraj Gurung, Daniel Laney, Peter Lindstrom, Jarek Rossignac, Squad: Compact representation for triangle meshes, Comput. Graph. Forum 30 (2) (2011) 355–364.

[5] J.F. Remacle, J. Lambrechts, B. Seny, E. Marchandise, A. Johnen, C. Geuzainet, Blossom-quad: A non-uniform quadrilateral mesh generator using a minimum-cost perfect-matching algorithm, Internat. J. Numer. Methods Engrg. 89 (9) (2012) 1102–1119.

[6] Tarini Marco, Pietroni Nico, Cignoni Paolo, Panozzo Daniele, Puppo Enrico, Practical quad mesh simplification, Comput. Graph. Forum 29 (2) (2010) 407–418.

[7] Luiz Velho, Denis Zorin, 4-8 Subdivision, Elsevier Science Publishers B. V., 2001.

[8] Ioana Boier-Martin, Holly Rushmeier, Jingyi Jin, Parameterization of triangle meshes over quadrilateral domains, in: ACM International Conference Proceeding Series, 2004, pp. 193–203.

[9] Nathan A. Carr, Jared Hoberock, Keenan Crane, John C. Hart, Rectangular multi-chart geometry images, in: Eurographics Symposium on Geometry Processing, 2006, pp. 181–190.

[10] Jiazhil Xia, Ismael Garcia, Ying He, Shi Qing Xin, Gustavo Patow, Editable polycube map for gpu-based subdivision surfaces, in: Symposium on Interactive 3D Graphics and Games, 2011, pp. 151–158.

[11] Hongyu Wang, Miao Jin, Ying He, Xianfeng Gu, Hong Qin, User-controllable polycube map for manifold spline construction, in: ACM Symposium on Solid and Physical Modeling, Stony Brook, New York, Usa, 2008, pp. 397–404.

[12] Juncong Lin, Xiaogang Jin, Zhengwen Fan, Charlie C.L. Wang, Automatic polycube-maps, in: International Conference on Advances in Geometric Modeling and Processing, 2008, pp. 3–16.

[13] Ying He, Hongyu Wang, Chi Wing Fu, Hong Qin, A divide-and-conquer approach for automatic polycube map construction, Comput. Graph. 33 (3) (2009) 369–380.

[14] Shen Dong, Peer Timo Bremer, Michael Garland, Valerio Pascucci, John C. Hart, Spectral surface quadrangulation, in: ACM SIGGRAPH, 2006, pp. 1057–1066.

[15] Jin Huang, Muyang Zhang, Jin Ma, Xinguo Liu, Leif Kobbelt, Hujun Bao, Spectral quadrangulation with orientation and alignment control, ACM Trans. Graph. 27 (5) (2008) 1–9.

[16] Y. Tong, P. Alliez, D. Cohen-Steiner, M. Desbrun, Designing quadrangulations with discrete harmonic forms, in: Eurographics Symposium on Geometry Processing, Cagliari, Sardinia, Italy, 2006, pp. 201–210.

[17] Pierre Alliez, Bruno Lévy, Alla Sheffer, Nicolas Ray, Periodic global parameterization, ACM Trans. Graph. 25 (4) (2006) 1460–1485.

[18] Felix Kälberer, Matthias Nieser, Konrad Polthier, Quadcover – surface parameterization using branched coverings, Comput. Graph. Forum 26 (3) (2010) 375–384.

[19] Bruno Lévy, Yang Liu, Lp centroidal voronoi tessellation and its applications, ACM Trans. Graph. 29 (4) (2010) 1–11.

[20] Jonathan Palacios, Eugene Zhang, Rotational symmetry field design on surfaces, ACM Trans. Graph. 26 (3) (2007) 55.

[21] Wan-Chiu Li, Bruno Vallet, Nicolas Ray, Bruno Lévy, Representing higher-order singularities in vector fields on piecewise linear surfaces, IEEE Trans. Vis. Comput. Graphics 12 (5) (2006) 1315–1322.

[22] Nicolas Kowalski, Franck Ledoux, Pascal Frey, A pde based approach to multidomain partitioning and quadrilateral meshing, in: International Meshing Roundtable, 2013.

[23] T. Jiang, X. Fang, J. Huang, H. Bao, Y. Tong, M. Desbrun, Frame field generation through metric customization, ACM Trans. Graph. 34 (4) (2015) 1–11.

[24] Nicolas Ray, Dmitry Sokolov, Robust polylines tracing for n-symmetry direction field on triangulated surfaces, ACM Trans. Graph. (2014).

[25] Ryan Viertel, Braxton Osting, An approach to quad meshing based on harmonic cross-valued maps and the ginzburg-landau theory. 2017.

[26] Na Lei, Xiaopeng Zheng, Zhongxuan Luo, Feng Luo, Xianfeng Gu, Quadrilateral Mesh Generation II: Meromorphic Quartic Differentials and Abel-Jacobi Condition. arXiv preprint arXiv:1907.00216, 2019.

[27] Miao Jin, Junho Kim, Feng Luo, Xianfeng Gu, Discrete surface ricci flow, IEEE Trans. Vis. Comput. Graphics 14 (5) (2008) 1030–1043.

[28] Christophe Geuzaine, Jean-François Remacle, Gmsh: A 3-d finite element mesh generator with built-in pre- and post-processing facilities, Internat. J. Numer. Methods Engrg. 79 (11) (2009) 1309–1331.